Strangeness $S = -2$ baryon-baryon interactions in relativistic chiral effective field theory

Kai-Wen Li,[1,2] Tetsuo Hyodo,[2] and Li-Sheng Geng[1,3,*]

[1]School of Physics and Nuclear Energy Engineering and International Research Center for Nuclei and Particles in the Cosmos, Beihang University, Beijing 100191, China

[2]Yukawa Institute for Theoretical Physics, Kyoto University, Kyoto 606-8502, Japan

[3]Beijing Key Laboratory of Advanced Nuclear Materials and Physics, Beihang University, Beijing 100191, China

(Received 16 September 2018; published 26 December 2018)

We study the strangeness $S = -2$ baryon-baryon interactions in relativistic chiral effective field theory at leading order. Among the 15 relevant low-energy constants, 8 of them are determined by fitting to the state of the art lattice QCD data of the HAL QCD Collaboration (with $m_\pi = 146$ MeV), and the rest either are taken from the study of the $S = -1$ hyperon-nucleon systems, assuming strict SU(3) flavor symmetry, or are temporarily set equal to zero. Using the so-obtained low-energy constants, we extrapolate the results to the physical point and show that they are consistent with the available experimental scattering data. Furthermore, we demonstrate that the $\Lambda\Lambda$ and ΞN phase shifts near the ΞN threshold are very sensitive to the lattice QCD data fitted, to the pion mass, and to isospin symmetry-breaking effects. As a result, any conclusion drawn from lattice QCD data at unphysical pion masses (even close to the physical point) should be taken with caution. Our results at the physical point, similar to the lattice QCD data, show that a resonance (quasibound state) may appear in the $I = 0$ $\Lambda\Lambda$ (ΞN) channel.

DOI: 10.1103/PhysRevC.98.065203

I. INTRODUCTION

The strangeness $S = -2$ hyperon-nucleon (YN) and hyperon-hyperon (YY) interactions play a key role in many studies of great interest in hypernuclear physics and nuclear astrophysics, e.g., the existence of the H dibaryon and the Ξ hypernuclei, and the hyperon puzzle. Despite the large amount of experimental and theoretical efforts, the existence of the H dibaryon remains inconclusive (see, e.g., Refs. [1,2]). The H dibaryon was first predicted to exist by Jaffe [3] using the MIT bag model as a deeply bound six-quark state with strangeness $S = -2$, isospin $I = 0$, and spin-parity $J^P = 0^+$, appearing in the $^1S_0$ partial wave of the $\Lambda\Lambda$-ΞN-$\Sigma\Sigma$ coupled channels. Recent lattice QCD simulations performed at $m_\pi \gtrsim 389$ MeV showed some evidence for the existence of a bound H dibaryon below the $\Lambda\Lambda$ threshold [4–7]. However, subsequent studies have shown that when those results are extrapolated to the physical region the H dibaryon becomes either weakly bound or unbound [8–11]. Recently the HAL QCD Collaboration performed simulations very close to the physical region [2], namely, $m_\pi = 146$ MeV. Using the so-called HAL QCD method [12,13] and assuming SU(3) flavor symmetry, they obtained an effective $\Lambda\Lambda$-ΞN coupled-channel potential. The calculations using such a potential yielded a resonant state in the $\Lambda\Lambda$ channel (a quasibound state in the ΞN channel), which, however, showed sizable systematic uncertainties, depending on the evolution time t in their simulation. Furthermore, it was shown that the coupled-channel effects between $\Lambda\Lambda$ and ΞN are weak.

Regarding the existence of Ξ hypernuclei [14–16], a moderately attractive interaction was inferred from the $^{12}C(K^-, K^+)^{12}_{\Xi}Be$ reaction [17]. However, subsequent analyses showed that the Ξ potential could be attractive [17], almost vanishing [18], or weakly repulsive [19]. In 2015, the "KISO" event claimed a deeply bound Ξ^--^{14}N hypernucleus [20], indicating at least an attractive ΞN interaction. On the other hand, based on the few-body calculations of the ΞNN hypernucleus [21], a ΞNN bound state might appear, indicating that the ΞN interaction might be strongly attractive.

YN and YY interactions are important inputs to astrophysical studies as well, since hyperons might appear in the interior region of neutron stars. The inclusion of YN interactions results in a softening of the equation-of-state (EoS) of nuclear matter, which is inconsistent with the observations of two-solar-mass neutron stars [22,23], known as the "hyperon puzzle." In this case, repulsive YY interactions seem to provide one possible solution by stiffening the EoS [24,25].

In this work, we study the strangeness $S = -2$ YN and YY interactions in relativistic chiral effective field theory (ChEFT) at leading order (LO). It is an extension of our previous studies of the nucleon-nucleon (NN) [26,27] and strangeness $S = -1$ YN [28–31] systems. The relativistic ChEFT has been shown to be able to describe the NN, ΛN, and ΣN scattering data fairly well, already at LO [26–33]. In contrast to the $S = 0$ and $S = -1$ sectors, there are only a few experimental data in the $S = -2$ sector. Here we use the latest lattice QCD data of the HAL QCD Collaboration [2] to fix 8 of the 15 low-energy constants (LECs) at LO. The rest are determined from the $S = -1$ sector [29] assuming SU(3) flavor symmetry, or temporarily set equal to zero. In addition, we extrapolate the results to the physical region and compare

*lisheng.geng@buaa.edu.cn

them with the available $\Lambda\Lambda$ and ΞN experimental data. The consistency among the lattice QCD simulation, ChEFT, and experimental data is discussed.

The paper is organized as follows: In Sec. II we present a brief overview of the formalism of relativistic ChEFT. The fits to the lattice QCD data are discussed in Sec. III. Phase shifts, cross sections, and low-energy parameters for the $\Lambda\Lambda$, $\Sigma\Sigma$, and ΞN systems are shown in Sec. IV. We conclude with a short summary and outlook in Sec. V.

II. BARYON-BARYON INTERACTIONS IN RELATIVISTIC CHIRAL EFFECTIVE FIELD THEORY

ChEFT has been successfully applied to study low-energy (octet) baryon-baryon interactions [34–39] since the pioneering work of Weinberg [40,41]. Compared to phenomenological models, ChEFT has three main advantages. First, it has a deep connection with the underlying theory of the strong interactions, QCD, particularly, chiral symmetry and its breaking. Second, it employs a power counting scheme, which enables one to improve calculations systematically. As a result, one can estimate the uncertainty of the results. In addition, multibaryon forces can be treated on the same footing as two-body interactions. Recently, we explored a relativistic ChEFT approach to study the NN [26] and YN [29] interactions at LO, in which more relativistic effects were taken into account in the potentials and scattering equation than in the nonrelativistic ChEFT.

The main feature of the relativistic formalism is that the complete baryon spinors are retained in the calculations:

$$u_B(\boldsymbol{p}, s) = N_p \begin{pmatrix} 1 \\ \frac{\boldsymbol{\sigma}\cdot\boldsymbol{p}}{E_p+M_B} \end{pmatrix} \chi_s, \quad N_p = \sqrt{\frac{E_p + M_B}{2M_B}}, \tag{1}$$

where $E_p = \sqrt{\boldsymbol{p}^2 + M_B^2}$, and M_B is the averaged baryon mass. Apparently, Lorentz invariance is maintained by such a treatment. Details of the formalism can be found in Refs. [26,29].

For the strangeness $S = -2$ sector, the LO potentials consist of nonderivative four-baryon contact terms (CTs) and one-pseudoscalar-meson exchanges (OPMEs). Fifteen independent LECs appear in the CTs that have to be pinned down by fitting to either experimental or lattice QCD data. Strict SU(3) symmetry is imposed on the CTs and the coefficients of OPMEs, which can be found in, e.g., Refs. [37,38]. However, due to the mass difference of the exchanged mesons (π, K, η), SU(3) symmetry is broken in the OPMEs. We have followed the convention of Ref. [37] and our previous $S = -1$ work [29] to redefine the LECs such as $C_{1S0}^{\Lambda\Lambda}$, instead of using the SU(3) representation such as C_{1S0}^{27}. In addition to the 12 LECs already appearing in the $S = -1$ sector [29], 3 more (independent) LECs, defined as

$$V_{\rm CT}^{\Lambda\Lambda\to\Lambda\Lambda}(^1S_0) = \xi_B\big[C_{1S0}^{4\Lambda}\big(1 + R_p^2 R_{p'}^2\big) + \hat{C}_{1S0}^{4\Lambda}\big(R_p^2 + R_{p'}^2\big)\big], \tag{2}$$

$$V_{\rm CT}^{\Lambda\Lambda\to\Lambda\Lambda}(^3P_1) = \xi_B\big(-\tfrac{4}{3}C_{3P1}^{4\Lambda} R_p R_{p'}\big), \tag{3}$$

appear in the $S = -2$ sector. Here $\xi_B = N_p^2 N_{p'}^2$, $R_p = |\boldsymbol{p}|/(E_p + M_B)$, and $R_{p'} = |\boldsymbol{p}'|/(E_{p'} + M_B)$. To obtain the scattering amplitude $T_{\rho\rho'}^{\nu\nu',J}$, the coupled-channel Kadyshevsky equation is solved:

$$T_{\rho\rho'}^{\nu\nu',J}(p', p; \sqrt{s}) = V_{\rho\rho'}^{\nu\nu',J}(p', p) + \sum_{\rho'',\nu''} \int_0^\infty \frac{dp'' p''^2}{(2\pi)^3} \frac{M_{B_{1,\nu''}} M_{B_{2,\nu''}}\, V_{\rho\rho''}^{\nu\nu'',J}(p', p'')\, T_{\rho''\rho'}^{\nu''\nu',J}(p'', p; \sqrt{s})}{E_{1,\nu''} E_{2,\nu''}(\sqrt{s} - E_{1,\nu''} - E_{2,\nu''} + i\epsilon)}, \tag{4}$$

where $V_{\rho\rho'}^{\nu\nu',J}$ is the interaction kernel which consists of CTs and OPMEs, $\sqrt{s}$ is the total energy of the baryon-baryon system in the center-of-mass frame, and $E_{n,\nu''} = \sqrt{\boldsymbol{p}''^2 + M_{B_{n,\nu''}}^2}$ ($n = 1$ and 2), where $M_{B_{n,\nu''}}$ are the baryon masses in the intermediate state. The labels ρ, ρ', and ρ'' denote the partial waves, and ν, ν', and ν'' denote the particle channels. The Coulomb interaction is not considered in the present work due to the lack of near-threshold data and because it would require a complicated treatment. This is consistent with the lattice QCD simulations [2]. To avoid ultraviolet divergence in solving the scattering equation, the chiral potentials are multiplied by an exponential form factor,

$$f_{\Lambda_F}(p, p') = \exp\left[-\left(\frac{p}{\Lambda_F}\right)^4 - \left(\frac{p'}{\Lambda_F}\right)^4\right], \tag{5}$$

with a cutoff value of $\Lambda_F = 600$ MeV.[1] Note that the cutoff function is not yet in an explicitly covariant form. For a relevant discussion, see, e.g., Refs. [26,27].

III. A FIT TO THE LATTICE QCD RESULTS

Recently the HAL QCD Collaboration performed simulations for the strangeness $S = -2$ baryon-baryon systems with almost physical pion masses ($m_\pi = 146$ MeV) [2]. The so-called HAL QCD approach [12,13] is employed to extract the

[1]We have chosen the value of Λ_F that can best describe the strangeness $S = -1$ YN scattering data [29], though acceptable fits to the data can be obtained with a cutoff ranging from 550 to 800 MeV in that sector (see Ref. [31] for more discussions). We leave a careful study of the cutoff dependence of the results in the $S = -2$ sector to a future study once more precise data become available.

TABLE I. Lattice QCD data used in the fits and the corresponding independent LECs of the relativistic ChEFT approach.

Reaction	I	Partial wave	Phase shifts	Corresponding LECs
$\Sigma\Sigma \to \Sigma\Sigma$	2	${}^1S_0$	$E_{\text{c.m.}} \leqslant 40$ MeV [42]	$C^{\Sigma\Sigma}_{1S0}$, $\hat{C}^{\Sigma\Sigma}_{1S0}$
$\Xi N \to \Xi N$	0	${}^3S_1$	$E_{\text{c.m.}} \leqslant 40$ MeV [42]	C^{8a}_{3S1}, $\hat{C}^{8a}_{3S1}$
$\Lambda\Lambda \to \Lambda\Lambda$	0	${}^1S_0$	$E_{\text{c.m.}} \leqslant 20$ MeV, 32 MeV $\leqslant E_{\text{c.m.}} \leqslant 32.8$ MeV [2]	
$\Xi N \to \Xi N$	0	${}^1S_0$	$32 \leqslant E_{\text{c.m.}} \leqslant 32.8$ MeV [2]	$C^{\Lambda\Lambda}_{1S0}$, $\hat{C}^{\Lambda\Lambda}_{1S0}$, $C^{4\Lambda}_{1S0}$, $\hat{C}^{4\Lambda}_{1S0}$
Inelasticity	0	${}^1S_0$	$32 \leqslant E_{\text{c.m.}} \leqslant 32.8$ MeV [2]	

potentials from the Nambu-Bethe-Salpeter wave functions on the lattice. Although the resulting potentials should in principle be independent of the measured time slice t, current results show sizable dependence on the evolution time t, which should be regarded as the systematic uncertainty of the lattice QCD simulation [42]. They obtained results for the $I = 2$ $\Sigma\Sigma$ ${}^1S_0$ phase shifts, the $I = 0$ ΞN ${}^3S_1$ phase shifts [42], the $I = 0$ $\Lambda\Lambda$ phase shifts, the ΞN ${}^1S_0$ phase shifts, and the inelasticity [2] using the effective $\Lambda\Lambda$-ΞN coupled channels, instead of the full $\Lambda\Lambda$-ΞN-$\Sigma\Sigma$ coupled channels.

In the present work, we fit these lattice QCD data [2,42] to determine the relevant eight LECs of the CTs. The fits are performed in the following steps.[2]

First, we fit to the lattice QCD $I = 2$ $\Sigma\Sigma$ ${}^1S_0$ phase shifts with the center-of-mass energy $E_{\text{c.m.}} \leqslant 40$ MeV, where $E_{\text{c.m.}} = \sqrt{s} - M_{B_1} - M_{B_2}$. M_{B_1} and M_{B_2} are the baryon masses of the channel with the lowest energy threshold. This is a single-channel scattering and the two LECs $C^{\Sigma\Sigma}_{1S0}$ and $\hat{C}^{\Sigma\Sigma}_{1S0}$ can be fixed. All results with $t = 11$–13 were used to estimate the central value and the uncertainty of the phase shift at each energy.

Second, the ${}^3S_1$ partial wave of the $I = 0$ ΞN system is treated in the same way. Note that in our convention the relevant LECs are defined as

$$\begin{aligned} V^{\Xi N\to\Xi N}_{\text{CT},I=0}({}^3S_1) &= \xi_B\left[\tfrac{1}{9}\left(C^{\Lambda\Lambda}_{3S1} - C^{\Lambda\Sigma}_{3S1}\right)\left(9 + R_p^2 R_{p'}^2\right)\right. \\ &\quad \left. + \tfrac{1}{3}\left(\hat{C}^{\Lambda\Lambda}_{3S1} - \hat{C}^{\Lambda\Sigma}_{3S1}\right)\left(R_p^2 + R_{p'}^2\right)\right] \\ &= \xi_B\left[\tfrac{1}{9}C^{8a}_{3S1}\left(9 + R_p^2 R_{p'}^2\right) + \tfrac{1}{3}\hat{C}^{8a}_{3S1}\left(R_p^2 + R_{p'}^2\right)\right]. \end{aligned} \tag{6}$$

In this case only the two combinations of those four relevant LECs can be pinned down, namely, C^{8a}_{3S1} and $\hat{C}^{8a}_{3S1}$. For the LECs (or the combinations of LECs) that contribute to the SU(3) structures 10 and 10^* in the ${}^3S_1$ partial waves, we have taken their values from the $S = -1$ sector via SU(3) symmetry [29].

Six LECs appear in the spin-singlet $\Lambda\Lambda$-ΞN-$\Sigma\Sigma$ coupled channels, $C^{\Sigma\Sigma}_{1S0}$, $\hat{C}^{\Sigma\Sigma}_{1S0}$, $C^{\Lambda\Lambda}_{1S0}$, $\hat{C}^{\Lambda\Lambda}_{1S0}$, $C^{4\Lambda}_{1S0}$, and $\hat{C}^{4\Lambda}_{1S0}$, but two of them, $C^{\Sigma\Sigma}_{1S0}$ and $\hat{C}^{\Sigma\Sigma}_{1S0}$, have been fixed from the $I = 2$ $\Sigma\Sigma$ ${}^1S_0$ phase shifts as described above. Unlike the $I = 2$ $\Sigma\Sigma$ ${}^1S_0$ and $I = 0$ ΞN ${}^3S_1$ cases, the lattice QCD data on the $I = 0$ $\Lambda\Lambda$ and ΞN phase shifts obtained at various time t look rather different. A resonant $\Lambda\Lambda$ state (a quasibound ΞN state below the threshold) is found with the $t = 9$, 10, and 11 lattice QCD data, but not with the $t = 12$ data. Therefore, we have performed separate fits to the lattice QCD data obtained at different t ranging from 9 to 12. The low-energy $\Lambda\Lambda$ ${}^1S_0$ phase shifts with $E_{\text{c.m.}} \leqslant 20$ MeV, the $\Lambda\Lambda$ and ΞN phase shifts, and the inelasticity with $32 \leqslant E_{\text{c.m.}} \leqslant 32.8$ MeV are taken into account. Because the ΞN quasibound state appears very close to the ΞN threshold at $E_{\text{c.m.}} = 32$ MeV with $m_\pi = 146$ MeV, the near-threshold data are included.

We summarize the details of the lattice QCD data used and the corresponding LECs in Table I. The values of the S-wave LECs are listed in Table II. The LEC $C^{4\Lambda}_{3P1}$ in the ${}^3P_1$ partial wave of the $\Lambda\Lambda \to \Lambda\Lambda$ reaction is not determined by this analysis, but it contributes to the $\Lambda\Lambda$- and $\Xi^- p$-induced cross sections. We temporarily set $C^{4\Lambda}_{3P1} = 0$ for the calculation of the cross section, assuming that the low-energy cross section is dominated by the S-wave contribution.

IV. RESULTS AND DISCUSSION

A. The $I = 2$ $\Sigma\Sigma$ ${}^1S_0$ phase shifts

In Fig. 1, we show the $I = 2$ $\Sigma\Sigma$ ${}^1S_0$ phase shifts. The dashed lines are the fitted results with $m_\pi = 146$ MeV. We obtained a $\chi^2/\text{DOF} = 0.08$ after the fits, which indicates a good description of the lattice QCD data. The solid lines are the extrapolations to the physical pion mass, with the isospin symmetry being assumed for the hadron masses. The extrapolations were done by only changing the hadron masses to their physical values, but keeping the coupling constants F, D, and f_0 and the other LECs fixed.

TABLE II. LECs for the S-wave contact terms (in units of 10^4 GeV^{-2}). The ${}^3S_1$ LECs are decomposed with the help of the $S = -1$ scattering data [29], assuming SU(3) symmetry.

	$C^{\Sigma\Sigma}_{1S0}$	$\hat{C}^{\Sigma\Sigma}_{1S0}$	$C^{\Lambda\Lambda}_{1S0}$	$\hat{C}^{\Lambda\Lambda}_{1S0}$	$C^{4\Lambda}_{1S0}$	$\hat{C}^{4\Lambda}_{1S0}$
	−0.0418	0.1726				
$t = 9$			−0.0154	0.0041	−0.0088	0.3570
$t = 10$			−0.0183	0.0977	−0.0134	0.6544
$t = 11$			−0.0202	−0.0482	−0.0038	0.8982
$t = 12$			0.0157	0.6119	0.1709	−0.1982
	$C^{\Lambda\Lambda}_{3S1}$	$\hat{C}^{\Lambda\Lambda}_{3S1}$	$C^{\Sigma\Sigma}_{3S1}$	$\hat{C}^{\Sigma\Sigma}_{3S1}$	$C^{\Lambda\Sigma}_{3S1}$	$\hat{C}^{\Lambda\Sigma}_{3S1}$
	0.0137	0.9261	0.0872	−0.4132	0.0230	0.2880

[2]The relevant masses and coupling constants are fixed at $m_\pi = 146$ MeV, $m_K = 525$ MeV, $m_N = 958$ MeV, $m_\Lambda = 1140$ MeV, $m_\Sigma = 1223$ MeV, and $m_\Xi = 1354$ MeV [2]. In addition, we have used $D + F = g_A = 1.277$, $F/(F + D) = 0.4$, and $f_0 \simeq f_\pi = 92.2$ MeV [29].

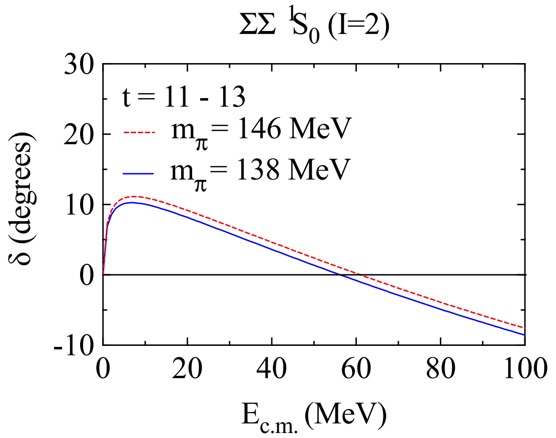

FIG. 1. Phase shifts of the $I = 2$ $\Sigma\Sigma$ $^1S_0$ partial wave. The dashed line denotes the result with $m_\pi = 146$ MeV and the solid line denotes the result with $m_\pi = 138$ MeV.

For the $\Sigma\Sigma$ $^1S_0$ channel, the phase shifts at the low-energy region are positive, indicating that the attractions are weak, but at the high-energy region the interactions become repulsive. In the SU(3) basis, the $^1S_0$ partial waves of $\Sigma\Sigma$ ($I = 2$), ΣN ($I = 3/2$), and NN ($I = 1$) all belong to the same representation of 27. However, the maximum value of the phase shifts are about 10° for the $\Sigma\Sigma$ system, 40° for the ΣN system [29], and 60° for the NN system [26]. This clearly tells us that the 27 SU(3) representation is becoming less attractive with the increase of the strangeness. On the other hand, we checked that a simultaneous fit of the $\Sigma^+ p$ cross sections and the lattice $\Sigma\Sigma$ $^1S_0$ phase shifts failed, similar to the attempt at a combined fit of NN and strangeness $S = -1$ YN data [29]. As a result, we conclude that SU(3) symmetry-breaking effects should be included if one wishes to simultaneously describe the systems with different strangeness, as also discussed in Ref. [38]. We note that the extrapolation to the physical point only causes minor changes of the phase shifts.

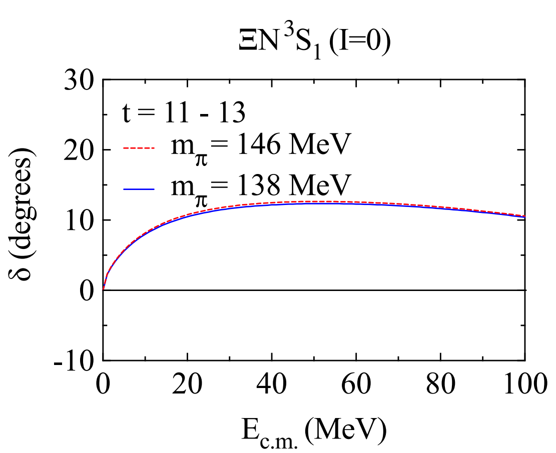

FIG. 2. Phase shifts of the $I = 0$ ΞN $^3S_1$ partial wave. The dashed line denotes the result with $m_\pi = 146$ MeV and the solid line denotes the result with $m_\pi = 138$ MeV.

B. The $I = 0$ ΞN $^3S_1$ phase shifts

The ΞN $^3S_1$ phase shifts are shown in Fig. 2, with a fitted $\chi^2/\mathrm{DOF} = 2.68$. The relativistic ChEFT can describe the low-energy lattice data well, but not those of high energies. Namely, lattice data show that the phase shift turns negative at high energies [42], which is not reproduced in the present study. It seems that higher-order chiral potentials are needed in this channel to provide enough repulsion at high energies.

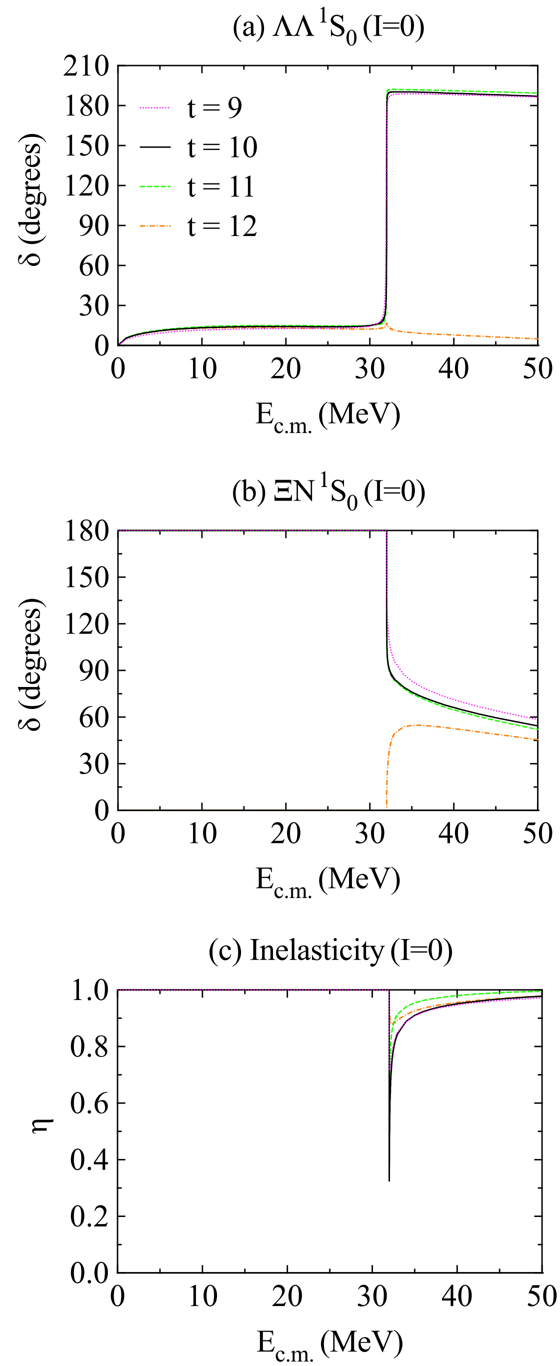

FIG. 3. $I = 0$ $\Lambda\Lambda$ and ΞN $^1S_0$ phase shifts and the inelasticity with $m_\pi = 146$ MeV and $t = 9$–12. The inelasticity η is defined as $S_{ii} = \eta e^{2i\delta_i}$.

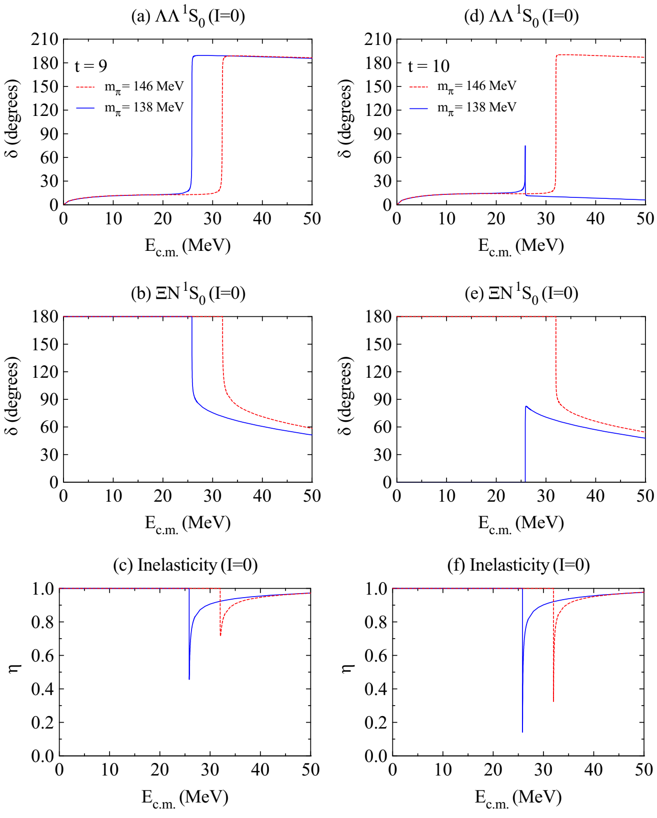

FIG. 4. $I = 0$ $\Lambda\Lambda$ and ΞN $^1S_0$ phase shifts and the inelasticity with $m_\pi = 146$ MeV (dashed lines) and $m_\pi = 138$ MeV (solid lines) and with $t = 9$ (a–c) and $t = 10$ (d–f).

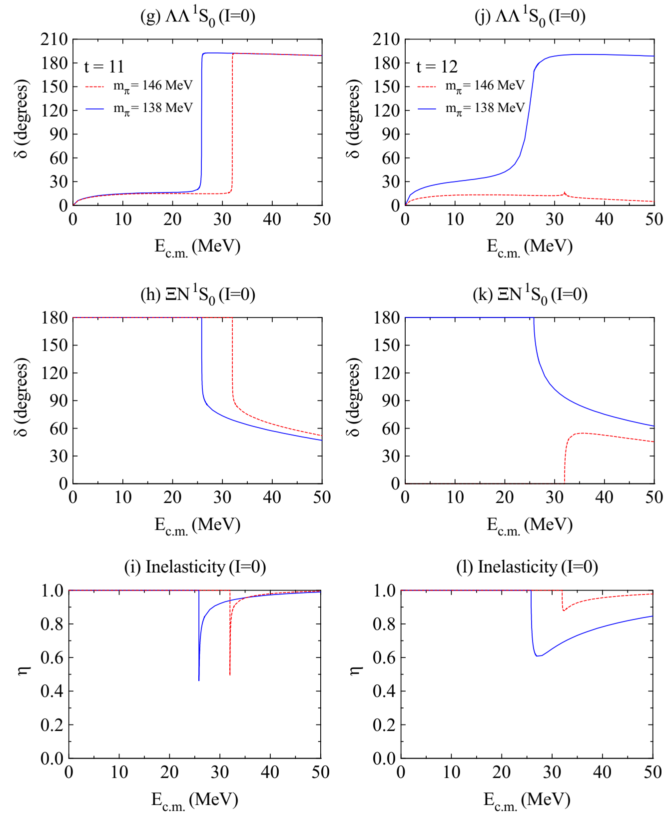

FIG. 5. $I = 0$ $\Lambda\Lambda$ and ΞN $^1S_0$ phase shifts and the inelasticity with $m_\pi = 146$ MeV (dashed lines) and $m_\pi = 138$ MeV (solid lines) and with $t = 11$ (g–i) and $t = 12$ (j–l).

In this channel, the phase shifts remain almost the same after the chiral extrapolation to the physical point as well.

C. The $\Lambda\Lambda$-ΞN-$\Sigma\Sigma$ $^1S_0$ phase shifts

As for the $\Lambda\Lambda$-ΞN-$\Sigma\Sigma$ coupled-channel, which is important for the study of the H dibaryon, we can obtain a good description of the lattice QCD data on the $\Lambda\Lambda$ and ΞN phase shifts and the inelasticity for each $t = 9$, 10, 11, and 12, with the corresponding $\chi^2/\mathrm{DOF} = 0.42$, 0.11, 0.30, and 0.01, respectively. The results are shown in Fig. 3. The sharp resonant state of $\Lambda\Lambda$ (the quasibound state of ΞN) is well reproduced for $t = 9$–11. However, the extrapolations to the physical pion mass look quite different for $t = 9$–12, as shown in Figs. 4 and 5. The sharp resonance remains with $t = 9$ and $t = 11$, but it disappears with $t = 10$. For the case of $t = 12$, a quasibound state appears in the ΞN system after the extrapolation, while the quasibound state is absent at $m_\pi = 146$ MeV. Note that the ΞN threshold has changed after the extrapolation, because the baryon masses changed as well. The origin of this difference of the extrapolation is discussed in Sec. IV D. We have also calculated the $\Lambda\Lambda$ scattering lengths in the physical region with $t = 9$–12 and found that they are consistent with the analyses from the hypernuclear experiments and the analysis of the two-particle correlations in heavy-ion collisions [43–54], as shown in Table III.

D. The ΞN quasibound state

Our above study showed that the existence of the ΞN quasibound state (the H dibaryon) is a quite delicate issue. To understand the different behavior of the extrapolation, we show the inverse of the $^1S_0$ scattering length of the ΞN channel multiplied with i, i.e., $i/a_{\Xi N}$, in Fig. 6. Because ΞN is not the coupled channel with the lowest threshold, the scattering length $a_{\Xi N}$ is, in general, complex due to the decay to the $\Lambda\Lambda$ channel. When $|a_{\Xi N}|$ is much larger than the typical length scale of the strong interaction $\sim$1 fm, $i/a_{\Xi N}$ represents approximately the pole position of the ΞN scattering amplitude in the complex momentum plane. If Im $(i/a_{\Xi N}) > 0$, then the pole is in the first Riemann sheet of the complex energy plane, indicating that the ΞN system has a quasibound state.

One can see that for $t = 9$ and 10, the evolution from $m_\pi = 146$ MeV to the physical pion mass is similar. The value of the imaginary part decreases and finally becomes negative

TABLE III. Physical $\Lambda\Lambda$ $^1S_0$ scattering length with $t = 9$–12 (in units of fm).

	$t = 9$	$t = 10$	$t = 11$	$t = 12$	Expt. analyses [43–54]
$a^{\Lambda\Lambda}_{1S0}$	-0.49	-0.60	-0.67	-1.44	$-1.87 \sim -0.5$

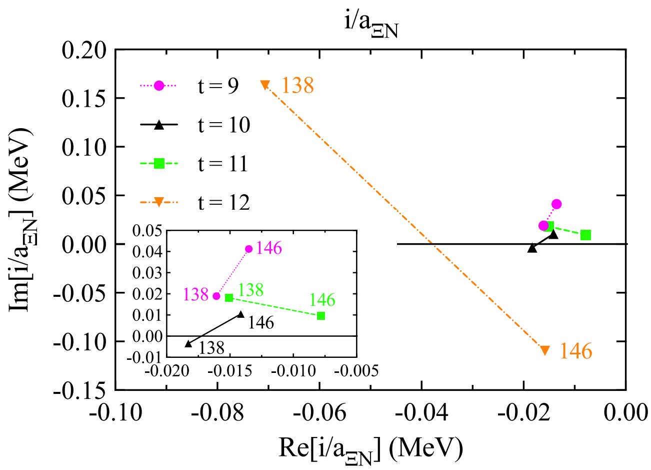

FIG. 6. Inverse of the $^1S_0$ scattering length of the $I = 0$ ΞN channel as a function of the pion mass.

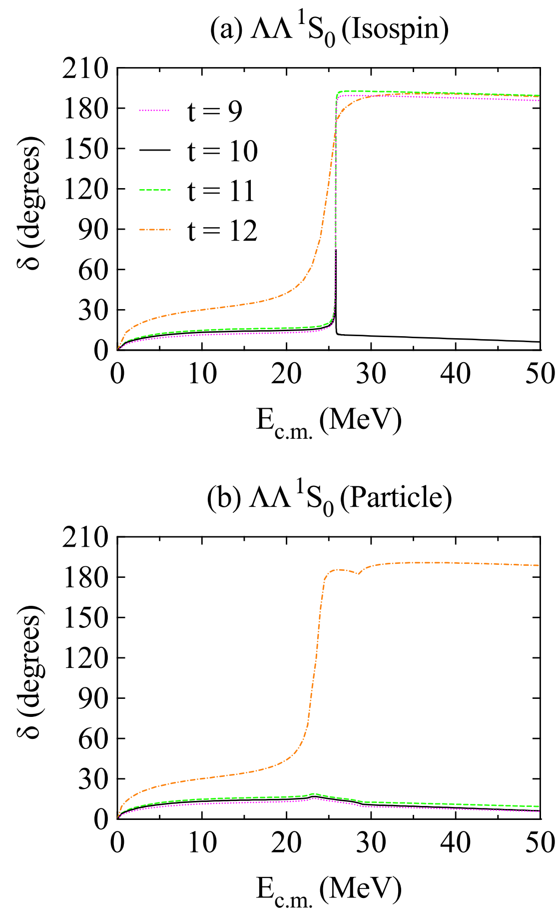

FIG. 7. $\Lambda\Lambda$ $^1S_0$ phase shifts with isospin-averaged baryon masses (a) and with physical baryon masses (b).

for $t = 10$ when extrapolated to the physical region, which corresponds to the disappearance of the quasibound state in the ΞN system. Im $(i/a_{\Xi N}) < 0$ indicates that the pole is in the second Riemann sheet of the ΞN channel, which is not the most adjacent sheet to the physical scattering axis, and hence the structure is not directly visible in observables. While for $t = 11$ and 12, the trend is the opposite. In both cases, the imaginary part of $i/a_{\Xi N}$ increases, and a quasibound state appears in the physical region. Especially for $t = 12$, the scale of the movement is relatively larger compared with the other three cases. Such a behavior originates from the values of the LECs with $t = 12$, e.g., the magnitudes of $\hat{C}^{\Lambda\Lambda}_{1S0}$ and $C^{4\Lambda}_{1S0}$ are larger than those with $t = 9$–11, as shown in Table II. In this way, the fate of the quasibound state in the extrapolation procedure is very sensitive. Even small changes of the inverse scattering length at $m_\pi = 146$ MeV can result in completely different behavior at the physical point.

The above calculations are performed in the isospin basis, where it is a $\Lambda\Lambda$-ΞN-$\Sigma\Sigma$ coupled channel with a common baryon mass being used for each isospin multiplet. If we consider isospin symmetry-breaking effects in the baryon masses, we should calculate them in the $\Lambda\Lambda$-$\Xi^0 n$-$\Xi^- p$-$\Sigma^0\Lambda$-$\Sigma^0\Sigma^0$-$\Sigma^-\Sigma^+$ coupled channels. In Fig. 7 we compare the $\Lambda\Lambda$ $^1S_0$ phase shifts obtained with or without isospin symmetry for the baryon masses. Note that with the physical baryon masses, the threshold energy of $\Xi^0 n$ is different from that of $\Xi^- p$, and there appear two threshold cusps around $E_{\text{c.m.}} \approx 25$ MeV. It can be seen that those sharp resonant states have disappeared if the isospin symmetry-breaking effects are included. Only for the $t = 12$ case does the resonant state appear at the $\Xi^0 n$ threshold, which corresponds to a quasibound state of the $\Xi^0 n$ system.

We summarize the different scenarios for the existence of a ΞN bound state in Table IV. The results are based on the fits to the central values of the lattice QCD data. It can be seen that the quasibound state in the ΞN system is extremely sensitive to the lattice QCD data fitted, to the pion mass, and to the isospin symmetry-breaking effects. We note that the strong sensitivity of the behavior of the phase shift around the ΞN threshold with respect to the isospin symmetry-breaking effect was also discussed in Ref. [38]. However, the $\Lambda\Lambda$ scattering length remains almost the same with or without isospin symmetry-breaking effects taken into account.

In our study, we have also taken into account the statistical errors of the lattice QCD results. In principle, the lattice QCD simulations are more reliable as the time t increases, but the uncertainties increase as well. To balance reliability and accuracy, we chose the case of $t = 10$ to study the extrapolations taking into account uncertainties. The previous fits were performed using the central values of the ΞN lattice QCD phase shifts with $32 \leqslant E_{\text{c.m.}} \leqslant 32.8$ MeV. We have also fitted to the upper bound and lower bound of the lattice QCD results of the ΞN channel.[3] The near-threshold ΞN phase shifts at $m_\pi = 146$ MeV, at the physical point and the extrapolations of $i/a_{\Xi N}$ for all the three cases are shown in Fig. 8. These results show that as the ΞN $^1S_0$ phase shifts at $m_\pi = 146$ MeV decrease, the slope of the trajectories with the extrapolation becomes smaller. In particular, if we use the lower bound of the ΞN lattice QCD phase shifts at $t = 10$, the quasibound state survives in the physical region.

[3]Please refer to Fig. 2(b) of Ref. [2].

TABLE IV. Summary of the ΞN quasibound state in different scenarios. The big circle ◯ represents the existence of the quasibound state.

Lattice data	$t = 9$	$t = 10$	$t = 11$	$t = 12$
$m_\pi = 146$ MeV	◯	◯	◯	
$m_\pi = 138$ MeV with isospin-averaged baryon masses	◯		◯	◯
Physical hadron masses				◯

E. Cross sections and low-energy parameters

Finally we compare our results with the available experimental data. We note that the cross sections calculated using the relevant LECs determined with the $t = 9$ and $t = 10$ lattice QCD data are more consistent with their experimental counterparts than those obtained with the $t = 11$ and $t = 12$ lattice QCD data. Following the preceding paragraph, we study the case of $t = 10$ in this sector. In Fig. 9, we show the $\Lambda\Lambda$- and $\Xi^- p$-induced cross sections with the statistical errors discussed previously taken into account. The cross sections are calculated with all the partial waves with total angular momentum $J \leqslant 2$. The experimental data are taken from Refs. [55,56]. One can see that our results are consistent with the scattering data, although the latter has a sizable uncertainty. Such a comparison shows that the lattice QCD data (in particular, those obtained with $t = 10$), the relativistic ChEFT approach, and the experimental data are in general consistent with each other.

In Table. V, we summarize the scattering lengths and effective ranges for various channels with the LECs determined by fitting to the $t = 10$ lattice QCD data. For the sake of comparison, we show as well the next-to-leading order (NLO) and LO [37] heavy-baryon (HB) ChEFT [38] results obtained with a cutoff of $\Lambda_F = 600$ MeV, those of the NSC97f model [57], and those of the fss2 model [44]. Note that the Coulomb force is considered in the latter two approaches. The results from different approaches are rather scattered. Clearly, more experimental information is needed to further constrain the $S = -2$ baryon-baryon interactions.

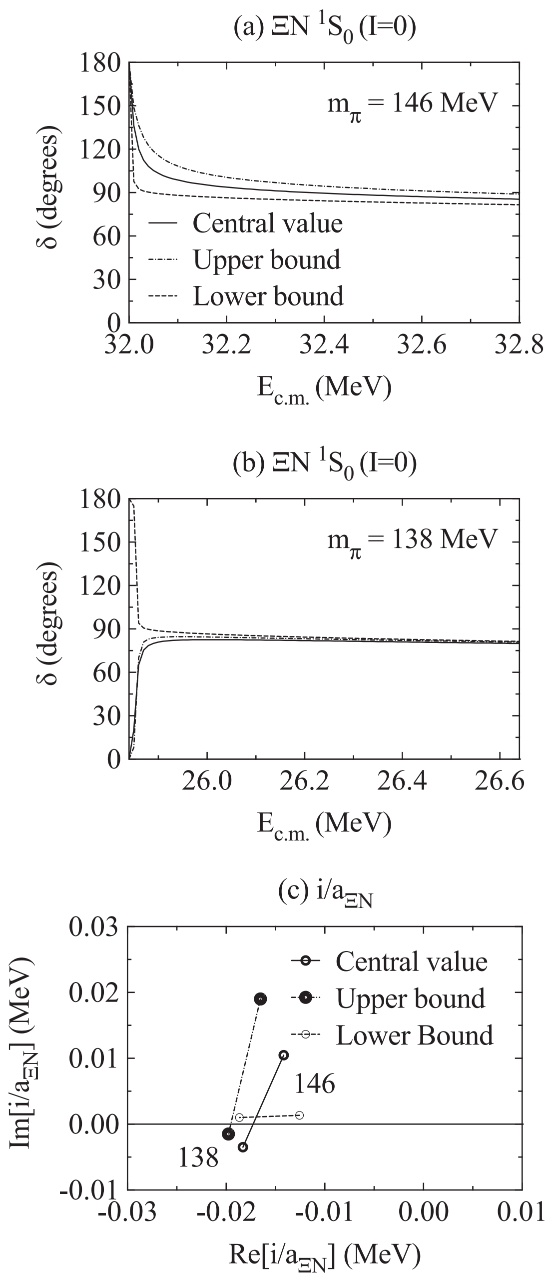

FIG. 8. Near-threshold ΞN $^1S_0$ phase shifts with $m_\pi = 146$ MeV (a), $m_\pi = 138$ MeV (b), and the extrapolations of $i/a_{\Xi N}$ (c) with $I = 0$ at $t = 10$ within the lattice QCD error bands.

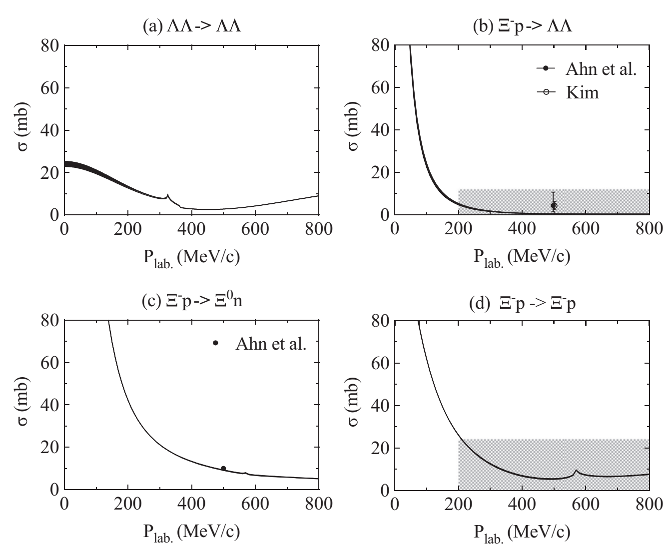

FIG. 9. $\Lambda\Lambda$- and $\Xi^- p$-induced cross sections with the LECs obtained by fitting to the $t = 10$ lattice QCD data. The experimental data are taken from Refs. [55,56]. The grid bands in $\Xi^- p \to \Lambda\Lambda$ and $\Xi^- p \to \Xi^- p$ reactions show the upper limits from Ref. [55]. $P_{\rm lab.}$ denotes for the laboratory momentum of Λ (a) or Ξ^- (b–d).

TABLE V. Predicted scattering lengths a and effective ranges r for various channels. The results obtained from HB ChEFT at NLO [38] and LO [37] with cutoff $\Lambda_F = 600$ MeV, the NSC97f model [57], and the fss2 model [44] are also shown for the sake of comparison. Note that the Coulomb force is considered in the latter two approaches.

Channel		This work	HB NLO [38]	HB LO [37]	NSC97f [57]	fss2 [44]
$\Sigma^+\Sigma^+$	$a_{1S0}^{\Sigma^+\Sigma^+}$	−0.80	−1.83	−7.76	6.98	−9.72
	$r_{1S0}^{\Sigma^+\Sigma^+}$	13.3	6.05	2.00	1.46	2.26
$\Xi^0 p$	$a_{1S0}^{\Xi^0 p}$	0.45	0.34	0.19	0.40	0.33
	$r_{1S0}^{\Xi^0 p}$	−4.55	−7.07	−37.7	−8.94	−9.23
	$a_{3S1}^{\Xi^0 p}$	−0.09	0.02	−0.00	−0.03	−0.20
	$r_{3S1}^{\Xi^0 p}$	72.5	1797	$>10^4$	912	27.4
$\Lambda\Lambda$	$a_{1S0}^{\Lambda\Lambda}$	−0.60	−0.66	−1.52	−0.35	−0.81
	$r_{1S0}^{\Lambda\Lambda}$	3.73	5.05	0.59	14.7	3.80
$\Xi^0 n$	$a_{3S1}^{\Xi^0 n}$	−0.14	−0.26	−0.25		
	$r_{3S1}^{\Xi^0 n}$	−14.0	5.26	−8.27		

It is interesting to compare our results with those of the NLO HB approach [38]. In particular, the scattering lengths of the $\Sigma^+\Sigma^+$ channel are rather different, but those of the $\Lambda\Lambda$ channel are quite similar, as shown in Table V. We note that in Ref. [38] they have fitted to the pp phase shifts and the $\Sigma^+ p$ cross sections to fix the relevant LECs in the S-wave contact terms with SU(3) symmetry-breaking effects taken into account and then made predictions for the $\Sigma^+\Sigma^+$ channel. Our study shows that the lattice QCD data seem to prefer a $\Sigma^+\Sigma^+$ attraction weaker than that predicted by the NLO HB approach, indicating that the suppression of the attraction as one adds more strangeness into the system may be larger than that considered in Ref. [38] (see also the discussion in Sec. IV A). Note that our results for the $\Sigma^+\Sigma^+$ channel are not dependent on t. On the other hand, the similar results for the $\Lambda\Lambda$ channel can be easily understood. The NLO HB approach fixed the relevant LECs by the empirical value of the $\Lambda\Lambda$ scattering length within the range of $-1 \sim -0.5$ fm, while our fits to the lattice QCD data also yield a $a_{1S0}^{\Lambda\Lambda}$ consistent with its empirical value (see Table III).

V. SUMMARY AND OUTLOOK

Recent progress in lattice QCD simulations provides us an unprecedented opportunity to better understand baryon-baryon interactions that play an important role in studies of hypernuclear and astronuclear physics. In particular, supplementary information on hyperon-nucleon(hyperon) interactions (to scarce experimental data) is key to understanding many important issues of current interest, such as the existence of H, ΩN [58], and $\Omega\Omega$ [59] dibaryons and the internal structure of neutron stars. Nevertheless, present lattice QCD simulations still suffer sizable systematic uncertainties originating from unphysical pion masses as well as coupled-channel effects. Careful studies of such effects are urgently needed to fully utilize the state-of-the-art lattice QCD simulations to advance our understanding of the nonperturbative strong interaction.

In the present work, we have studied the strangeness $S = -2$ baryon-baryon interactions in relativistic chiral effective field theory at leading order. The latest lattice QCD data of the HAL QCD Collaboration were used to fix the relevant low-energy constants. We obtained a good description of the lattice QCD results (with perhaps the exception of the high-energy $I = 0$ ΞN $^3S_1$ phase shifts). Extrapolations from $m_\pi = 146$ MeV to the physical region were made. The behavior of the ΞN system was found to be very sensitive to the lattice QCD data fitted. In addition, our results can describe the available experimental data very well, which show the overall consistency among lattice QCD simulations, the relativistic chiral effective field theory, and the experimental data.

ACKNOWLEDGMENTS

The authors are grateful to Kenji Sasaki for providing us with the latest lattice QCD results and a careful reading of this manuscript. K.W.L. and T.H. thank Wolfram Weise for useful discussions. This work is partly supported by the National Natural Science Foundation of China under Grants No.11522539 and No. 11735003, by the fundamental Research Funds for the Central Universities, by JSPS KAKENHI Grant No. JP16K17694, and by the Yukawa International Program for Quark-Hadron Sciences (YIPQS). K.W.L. acknowledges financial support from the China Scholarship Council.

[1] J. K. Ahn *et al.* (KEK-PS E224 Collaboration), Phys. Lett. B **444**, 267 (1998).

[2] K. Sasaki *et al.* (HAL QCD Collaboration), EPJ Web Conf. **175**, 05010 (2018).

[3] R. L. Jaffe, Phys. Rev. Lett. **38**, 195 (1977); **38**, 617(E) (1977).

[4] S. R. Beane, E. Chang, W. Detmold, B. Joo, H. W. Lin, T. C. Luu, K. Orginos, A. Parreno, M. J. Savage, A. Torok, and

A. Walker-Loud (NPLQCD Collaboration), Phys. Rev. Lett. **106**, 162001 (2011).
[5] T. Inoue, N. Ishii, S. Aoki, T. Doi, T. Hatsuda, Y. Ikeda, K. Murano, H. Nemura, and K. Sasaki (HAL QCD Collaboration), Phys. Rev. Lett. **106**, 162002 (2011).
[6] S. R. Beane, E. Chang, W. Detmold, H. W. Lin, T. C. Luu, K. Orginos, A. Parreno, M. J. Savage, A. Torok, and A. Walker-Loud (NPLQCD Collaboration), Phys. Rev. D **85**, 054511 (2012).
[7] A. Francis, J. R. Green, P. M. Junnarkar, C. Miao, T. D. Rae, and H. Wittig, arXiv:1805.03966.
[8] P. E. Shanahan, A. W. Thomas, and R. D. Young, Phys. Rev. Lett. **107**, 092004 (2011).
[9] J. Haidenbauer and U.-G. Meißner, Phys. Lett. B **706**, 100 (2011).
[10] T. Inoue *et al.* (HAL QCD Collaboration), Nucl. Phys. A **881**, 28 (2012).
[11] Y. Yamaguchi and T. Hyodo, Phys. Rev. C **94**, 065207 (2016).
[12] N. Ishii *et al.* (HAL QCD Collaboration), Phys. Lett. B **712**, 437 (2012).
[13] S. Aoki *et al.* (HAL QCD Collaboration), Prog. Theor. Exp. Phys. **2012**, 01A105 (2012).
[14] M. Yamaguchi, K. Tominaga, T. Ueda, and Y. Yamamoto, Prog. Theor. Phys. **105**, 627 (2001).
[15] E. Friedman and A. Gal, Phys. Rep. **452**, 89 (2007).
[16] E. Hiyama, M. Kamimura, Y. Yamamoto, T. Motoba, and T. A. Rijken, Prog. Theor. Phys. Suppl. **185**, 152 (2010).
[17] P. Khaustov *et al.* (AGS E885 Collaboration), Phys. Rev. C **61**, 054603 (2000).
[18] M. Kohno and S. Hashimoto, Prog. Theor. Phys. **123**, 157 (2010).
[19] Krishichayan, X. Chen, Y.-W. Lui, Y. Tokimoto, J. Button, and D. H. Youngblood, Phys. Rev. C **81**, 014603 (2010).
[20] K. Nakazawa *et al.*, Prog. Theor. Exp. Phys. **2015**, 033D02 (2015).
[21] H. Garcilazo and A. Valcarce, Phys. Rev. C **92**, 014004 (2015).
[22] P. Demorest, T. Pennucci, S. Ransom, M. Roberts, and J. Hessels, Nature (London) **467**, 1081 (2010).
[23] J. Antoniadis *et al.*, Science **340**, 1233232 (2013).
[24] D. Lonardoni, F. Pederiva, and S. Gandolfi, Phys. Rev. C **89**, 014314 (2014).
[25] K. A. Maslov, E. E. Kolomeitsev, and D. N. Voskresensky, Phys. Lett. B **748**, 369 (2015).
[26] X. L. Ren, K. W. Li, L. S. Geng, B. W. Long, P. Ring, and J. Meng, Chin. Phys. C **42**, 014103 (2018).
[27] X. L. Ren, K. W. Li, L. S. Geng, and J. Meng, arXiv:1712.10083.
[28] K. W. Li, X. L. Ren, L. S. Geng, and B. Long, Phys. Rev. D **94**, 014029 (2016).
[29] K. W. Li, X. L. Ren, L. S. Geng, and B. W. Long, Chin. Phys. C **42**, 014105 (2018).
[30] K. W. Li, X. L. Ren, L. S. Geng, and B. Long, PoS **INPC2016**, 276 (2017).
[31] J. Song, K. W. Li, and L. S. Geng, Phys. Rev. C **97**, 065201 (2018).
[32] X. L. Ren, K. W. Li, and L. S. Geng, Nucl. Phys. Rev. **34**, 392 (2017).
[33] X. L. Ren, K. W. Li, and L. S. Geng, arXiv:1709.10266.
[34] E. Epelbaum, H. W. Hammer, and U.-G. Meißner, Rev. Mod. Phys. **81**, 1773 (2009).
[35] R. Machleidt and D. R. Entem, Phys. Rep. **503**, 1 (2011).
[36] J. Haidenbauer, S. Petschauer, N. Kaiser, U.-G. Meißner, A. Nogga, and W. Weise, Nucl. Phys. A **915**, 24 (2013).
[37] H. Polinder, J. Haidenbauer, and U.-G. Meißner, Phys. Lett. B **653**, 29 (2007).
[38] J. Haidenbauer, U.-G. Meißner, and S. Petschauer, Nucl. Phys. A **954**, 273 (2016).
[39] J. Haidenbauer and U.-G. Meißner, Phys. Lett. B **684**, 275 (2010).
[40] S. Weinberg, Phys. Lett. B **251**, 288 (1990).
[41] S. Weinberg, Nucl. Phys. B **363**, 3 (1991).
[42] K. Sasaki (private communication).
[43] T. A. Rijken and Y. Yamamoto, Phys. Rev. C **73**, 044008 (2006).
[44] Y. Fujiwara, Y. Suzuki, and C. Nakamoto, Prog. Part. Nucl. Phys. **58**, 439 (2007).
[45] I. N. Filikhin and A. Gal, Nucl. Phys. A **707**, 491 (2002).
[46] I. R. Afnan and B. F. Gibson, Phys. Rev. C **67**, 017001 (2003).
[47] I. Filikhin, A. Gal, and V. M. Suslov, Nucl. Phys. A **743**, 194 (2004).
[48] T. Yamada, Phys. Rev. C **69**, 044301 (2004).
[49] I. Vidana, A. Ramos, and A. Polls, Phys. Rev. C **70**, 024306 (2004).
[50] Q. N. Usmani, A. R. Bodmer, and B. Sharma, Phys. Rev. C **70**, 061001 (2004).
[51] H. Nemura, S. Shinmura, Y. Akaishi, and K. S. Myint, Phys. Rev. Lett. **94**, 202502 (2005).
[52] A. M. Gasparyan, J. Haidenbauer, and C. Hanhart, Phys. Rev. C **85**, 015204 (2012).
[53] K. Morita, T. Furumoto, and A. Ohnishi, Phys. Rev. C **91**, 024916 (2015).
[54] L. Adamczyk *et al.* (STAR Collaboration), Phys. Rev. Lett. **114**, 022301 (2015).
[55] J. K. Ahn *et al.*, Phys. Lett. B **633**, 214 (2006).
[56] S. J. Kim, presentation at the 12th International Conference on Hypernuclear and Strange Particle Physics, Sendai, Japan, see http://lambda.phys.tohoku.ac.jp/hyp2015/, 2015.
[57] V. G. J. Stoks and T. A. Rijken, Phys. Rev. C **59**, 3009 (1999).
[58] T. Iritani *et al.*, arXiv:1810.03416.
[59] S. Gongyo, K. Sasaki, S. Aoki, T. Doi, T. Hatsuda, Y. Ikeda, T. Inoue, T. Iritani, N. Ishii, T. Miyamoto, and H. Nemura, Phys. Rev. Lett. **120**, 212001 (2018).